Carderock Division
Naval Surface Warfare Center
Bethesda, MD. 20084-5000

CARDIVNSWC-TR-601-93/02 July 1993
Survivability, Structures and Materials Directorate
Research and Development Report

Graphite/Polyurethane Flexible Composites - Mechanical and Vibration Damping Properties

by
Roger M. Crane
and
Colin Ratcliffe

CARDIVNSWC-TR-60-93/02 Graphite/Polyurethane Flexible Composites - Mechanical and Vibration Damping Properties

Carderock Division
Naval Surface Warfare Center
Bethseda, MD 20084-5000

CARDIVNSWC-TR-601-93/02 August 1993
Survivability, Structures and Materials Directorate
Research and Development Report

Graphite/Polyurethane Flexible Composites - Mechanical and Vibration Damping Properties

by
Roger M. Crane
Colin P. Ratcliffe

TABLE OF CONTENTS

	Page
LIST OF FIGURES	ii
LIST OF TABLES	iii
ABBREVIATIONS	iii
ABSTRACT	1
ADMINISTRATION INFORMATION	1
INTRODUCTION	1
FLEXIBLE COMPOSITE FABRICATION	4
MECHANICAL PROPERTY DETERMINATION	8
MECHANICAL VIBRATION DAMPING	14
DESIGN AND FABRICATION OF A FLEXIBLE COMPOSITE SHAFT COUPLING	20
MECHANICAL TESTING OF FLEXIBLE COMPOSITE SHAFT SECTION	29
AXIAL DAMPING TEST METHOD	39
THEORY	40
DAMPING RESULTS AND DISCUSSION	46
BASELINE STEEL SHAFT	47
BASELINE COMPOSITE SHAFT	49
FLEXIBLE COMPOSITE SHAFT - EMPTY	49
FLEXIBLE COMPOSITE SHAFT - SAND FILLED	50
LORD DAMPED COMPOSITE SHAFT	50
SENSITIVITY	51
CONCLUSIONS	52
ACKNOWLEDGEMENTS	54
REFERENCES	54
Appendix A Visual BASIC program to calculate accelerance of the pipe .	56

LIST OF FIGURES

FIGURE 1 Tensile Stress vs. Strain plot of Braided AS4/REN flexible composite 12

FIGURE 2 Tensile modulus as a function of strain for the AS4/polyurethane composite material. 13

FIGURE 3 Schematic of unit cell for braided fiber composite form 16

FIGURE 4 Damping loss factor of AS4 graphite braided composite with polyurethane matrix 17

FIGURE 5 Loss factor vs. mean cyclic stress for braided AS4 fiber with polyurethane matrix using phase lag analysis 19

FIGURE 6 Schematic of assembly used for epoxy resin transfer into braided preform 25

FIGURE 7 Closed mold used for polyurethane infiltration 27

FIGURE 8 Experimental apparatus used to torsionally load shaft sections 30

FIGURE 9 Torsional buckling of flexible shaft section loaded to 400 ft-lb... 31

FIGURE 10 Torsion test results of flexible coupling filled with sand..... 33

FIGURE 11 Failed coupling 35

FIGURE 12 Torsional test results of the second braided coupling 37

FIGURE 13 Coupling torsion test to failure 38

FIGURE 14 Free Body diagram for mass m_1 41

FIGURE 15 Overlay of the measured and theoretical frequency response functions for baseline steel shaft section 49

FIGURE 16 Overlay of the measured and theoretical frequency response functions for baseline composite shaft section 51

FIGURE 17 Overlay of the measured and theoretical frequency response functions for the flexible composite shaft section - empty 53

FIGURE 18 Overlay of the measured and theoretical frequency response functions for the flexible composite shaft section - sand filled 55

LIST OF TABLES

TABLE 1 Material properties of REN 7

TABLE 2 Mechanical properties of materials used in flexible composite specimens 10

TABLE 3 Material Properties of polyurethane 21

TABLE 4 Composite strength properties used in cylinder analysis 22

TABLE 5 Axial compression test results for damping tests on shaft sections 47

ABBREVIATIONS

°F	degrees Fahrenheit
FFT	Fast Fourier Transform
ft-lb	foot pounds
FRF	frequency response function
Hz	hertz
in	inch
in-lb	inch pounds
kg	kilo gram
kg/m^3	kilo gram per meter cubed
kHz	kilo hertz
ksi	thousand pounds per square inch
lb	pound
m	meter
min	minutes
Msi	million pounds per square inch
N	newton
N/m^2	newton per meter squared
PC	personal computer
psi	pounds per square inch
RTM	resin transfer molding

ABSTRACT

Structures fabricated with advanced composite materials, such as graphite fibers in thermoset or thermoplastic resins, typically possess high stiffness. The material is elastic to failure, which occurs at strain levels which are relatively low, on the order of 2 to 5 %, depending on fiber orientations. There are numerous naval applications in which systems are subjected to significantly large deformations due to the global deformation of the ship hull. To allow the subsystems to function while being subjected to these large global deformations, flexible couplings are often incorporated. These couplings must transfer in-plane loads and torque while allowing for dissimilar motion of each component. This paper describes such a structural configuration which is both flexible and structurally adequate to support significant mechanical loads. This flexible composite systems consists of a braided graphite fiber preform infiltrated with a polyurethane, Adiprene, which has a modulus of 1100 psi and a strain to failure of 300%. This composite system possesses adequate structural characteristics of strength and stiffness, the capability to undergo large global deformations, while simultaneously dissipating significant levels of mechanical vibration energy. This paper discusses the fabrication and design of the flexible composite material, the mechanical characteristics and the damping that it provides.

ADMINISTRATIVE INFORMATION

This project was financially supported by the Office of Naval Research, PE 62234N, Ship and Submarine Materials Block (SC2B) under the Work Unit 1-2802-606 for the initial materials investigation and under UN3A for preliminary investigation of flexible composites for shaft couplings.

INTRODUCTION

Composite materials are typically utilized in structural applications which require higher specific stiffness and strength than can be achieved with metals.

In addition, the consideration for the use of composite materials has been increasing for structures which also require a level of mechanical vibration damping greater than that possible with conventional structural metallic systems.

In general, for conventional structural materials, the characteristics of high stiffness and strength run opposite to high damping. Composite materials have the potential to possess both characteristics, since they are formed with two macroscopically distinct material components. Here, the structural component, the fiber, is combined with a less structural material, the matrix, which is typically a thermoset or thermoplastic polymer, to form a structure. These polymeric matrices have the material characteristics of being viscoelastic, where when they are loaded in a manner which varies sinusoidally with time, the deformations will lag the applied loads. Their dynamic material properties can therefore be described as having a stiffness, termed the storage modulus, and a quantity associated with the energy dissipated in each cycle, called the loss modulus. These characteristics are dependent on frequency and temperature. As a result of this viscoelastic property, the matrix has a damping loss factor which is typically 2 to 3 orders of magnitude greater than the loss factor of a structural metal. The damping loss factor of a composite which uses a polymeric material as its matrix will therefore possess a loss factor which is significantly greater than an equivalent metallic component.

The damping characteristics of organic matrix composite materials are primarily dependent on the damping characteristics the polymer system used. The viscoelastic properties of the matrix as it is loaded, as well as the shear

loading that occurs at the fiber/matrix interface, account for the majority of the energy dissipation in composites. In general, the greater the loss factor of the polymeric material, the greater the energy dissipation or damping loss factor of the composite.

In the design of structural components, the analyst is primarily concerned with the stress-strain behavior of specific material systems. If the additional requirement of weight reduction is imposed, composite materials become a primary material choice, because of their high specific stiffness and strength. The material suppliers, recognizing this, have typically concentrated on the development of composite systems which have increasing stiffness and strength. Little attention is normally given to the loss modulus of the matrix. It is the matrix stiffness and strength and fiber to matrix adhesion characteristics which are optimized in most circumstances.

High performance composite structures are generally manufactured using unidirectional aligned fibers in prepreg form, laminated with fiber orientations to support a given loading condition. To provide an optimum load transfer between fibers, a stiff, strong matrix is required. The matrix material is also the continuous phase of the composite system that enables the material to take on specific structural shapes. Other fiber forms have been developed, however, which without a matrix, maintain a given structural shape and impregnated with a structural matrix have mechanical properties which approach those achievable in unidirectional composites. One such material form is multidirectional through the thickness braided fiber preforms (1).

The through the thickness braided material possesses a structural integrity without matrix material because of the mechanical interaction that occurs between fibers as they progress throughout the material planform. The braiding process utilizes continuous fibers which are maneuvered so that they propagate through the thickness of the material as well as along the length of the structure, surfacing on all exterior surfaces of the part numerous times throughout the part length. The number of times that a particular fiber propagates through the thickness, as well as the specific apparent fiber orientation along the length of the structure are dependent on the specific braid parameters. Details of the process as well as the types of forms which can be fabricated using this type of material is presented in reference 1. Because of these characteristics, this fiber configuration can be used in conjunction with matrix materials having low stiffness to form a structure which is capable of supporting significant tensile loads.

Flexible Composite Fabrication

One class of material which possesses high damping is urethane rubber, commonly referred to as polyurethane. This material typically has a high elongation to failure, on the order of several hundred percent, and a damping loss factor, greater than 1.0. This magnitude of loss factor is typically at least an order of magnitude greater than conventional thermoset or thermoplastic resins which are used for composite construction. Since the matrix system of a composite provides the most significant contribution to the material damping, a composite fabricated with a polyurethane matrix should have a loss factor significantly greater than conventional composite systems.

A second characteristic that should occur in a fiber reinforced material with polyurethane matrix is large deformations when subjected to bending moments. This is especially desirable for misalignment couplings which are used as components of shafting or piping systems. The deformations in these flexible couplings would, however, have to be controllable. This could be accomplished by a design which would allow specific deformation to occur after which the fibers interact and transfer load through physical interactions. A multidimensional braided preform infiltrated with a polyurethane should provide these characteristics.

The initial objective of this program was to investigate the mechanical vibration damping characteristics of the braided composite impregnated with a highly viscoelastic material, such as a polyurethane or equivalent material system. In order to perform the damping tests and subsequent mechanical tests, initially the development of a methodology to impregnate the braided composite preform with the highly viscoelastic material needed to be developed.

The material form that was initially obtained was a through the thickness braided composite preform made using the AS4 graphite fiber. These initial braided preforms had a width of 2 inches. The braid pattern employed was a 3 x 1. This braid pattern resulted in an apparent surface fiber orientation of approximately $\pm 57°$. The braided preform had a thickness of approximately 0.125 in.

The braided preform was first cut to lengths of 9 inches. A closed mold was

fabricated using 0.5 in thick steel plates acting as the mold surfaces. Steel 0.5 in. bar stock was welded to form rectangular sections that were 9 x 2 in. This rectangular grid was then adhesively bonded to one of the steel plates using a high temperature RTV silicone rubber adhesive sealant. In order to achieve a specific final part thickness, a caul plate/spacer material of steel with dimensions 9 x 2 x 0.375 in. was fabricated. This spacer material had 0.0625 in holes drilled on 0.5 in. centers to allow for material flow out of the cavity.

The preform was placed in the mold cavity which was coated with a chemical release agent. The preliminary viscoelastic material used for this specimen form was REN. The material properties of this material are given in Table 1. The REN was then mixed and heated and poured into the mold cavity on top of the braided preform. The spacer plate was placed into the cavity and a top cover plate placed on top of this. The entire assembly was then placed into heated hydraulic press. The press plattens were closed until the top cover plate was in contact with the rectangular bar stock assembly. This assured that the thickness of the composite was 0.125 in. The entire assembly was kept in the press at a temperature of 150° F for 1 hour. The heat to the mold was then removed and the part was allowed to come to room temperature under pressure. Only one sample was fabricated using this technique.

After this sample was fabricated, it was mechanically tested in tension to determine the stiffness and strength of this system. Because of the softness of the composite sample, it was pulled out of the gripped regions when the load reached approximately 500 lb. This occurred using both wedge and hydraulic grips. Because of this, a modification to the above fabrication scheme was required.

Material Property	Experimental Value
E_1	1000 psi
E_2	1000 psi
ν_{12}	0.35
G_{12}	485 psi

Table 1 Material properties of REN

From the initial tensile tests, it became obvious that the areas of the braided material that would be gripped would need to have a greater stiffness through the thickness. This was accomplished by infiltrating the ends of the braided preform with a conventional epoxy . Initially, 2 inches of each end of the subsequent braided preforms were impregnated with Shell Epon 828 epoxy. This was done in a manner similar to that described above. The braided preform was first placed in the mold. The mold was placed in a slightly elevated vertical position. A specific volume of resin was measured and poured into the mold at the bottom end of the assembly. The spacer material was then placed on top and top cover plate clamped on top using C-clamps. The assembly was then placed vertically and allowed to remain in this position for 24 hours, to allow for full curing of the room temperature curing epoxy. When these epoxy infiltrated ends of the braided sample were gripped using either the wedge grips or the hydraulic grips, there was no slippage up to the failure load of the sample. This was the fabrication methodology that was used for the remainder of the braided composite preform samples.

Mechanical Property Determination

The braided composite preform infiltrated with the high elongation, compliant matrix is a material form for which no mechanical characteristics exist. Since this material form is to be utilized to damp mechanical vibrations as well as provide structural performance, the mechanical properties had to be determined.

There are well established analytical techniques available for estimating the stiffnesses of composite materials. For the braided composite which utilizes a conventional epoxy, the in-plane elastic moduli have been analytically determined using classical lamination theory (2). This type of analysis requires knowledge of the material stiffnesses, E_1, E_2, G_{12}, and ν_{12}. For conventional composite systems, these material properties can be analytically determined from knowledge of the material characteristics of the individual constituents, using the various micromechanical models that are available. This methodology was utilized to analytically determine the material characteristics of the braided graphite/REN composite.

The micromechanical models used to determine the elastic moduli of the flexible composite are the standard techniques utilized for traditional composite systems. Initially, the moduli of the fiber and matrix are required. The values utilized were manufacturers data. The properties are shown in Table 1. In addition, it is assumed that the fiber volume fraction for this composite system is 50%. With these values, the mechanical properties of the composite were determined.

For the determination of E_1, the rule of mixtures method was used. This method estimates the composite value of E_1 using the following equation

$$E_1 = E_f V_f + E_m V_m \tag{1}$$

where E_f and E_m are the moduli of the fiber and matrix, respectively, and V_f and V_m are the fiber volume fraction of the fiber and matrix, respectively. The fiber volume fraction used in the calculations is 50%. With the material constituents utilized, the inplane stiffness is calculated to be 17×10^6 psi.

To determine the transverse stiffness, the inverse rule of mixtures approach is utilized. The composite modulus, E_2, is determined from the constituent material transverse moduli with the relationship

$$\frac{1}{E_2} = \frac{V_f}{E_f} + \frac{V_m}{E_m} \tag{2}$$

where E_f, E_m, V_f and V_m have been previously defined above. For the constituent materials used in this effort, the composite transverse stiffness was analytically determined to be 2.0×10^3 psi.

The composite Poisson's ratio can be likewise determined using a rule of mixtures approach. As such, the composite Poisson's ratio is determined using the following equation

$$\nu_{12} = \nu_f V_f + \nu_m V_m \tag{3}$$

Using equation 3, the composite Poisson's ratio is determined to be 0.325.

The inplane shear modulus is determined using the inverse rule of mixtures approach. Specifically, the composite value of G_{12} is given as

$$\frac{1}{G_{12}} = \frac{V_f}{G_f} + \frac{V_m}{G_m} \tag{4}$$

For the specific material constituents use in this effort, the composite inplane shear modulus is determined to be 780 psi. The results of the micromechanical predictions are summarized in Table 2.

Property / Material	E_1 (psi)	E_2 (psi)	ν_{12}	G_{12} (psi)
AS4	34×10^6	3.0×10^6	0.3	4.0×10^6
REN	1.0×10^3	1.0×10^3	0.35	390
AS4/REN	17×10^6	2.0×10^3	0.325	780

Table 2 Mechanical properties of materials used in flexible composite specimens

It can be seen from Table 2 that the material properties other than E_1 are significantly less than conventional composite systems. For example, both E_2 and G_{12} are approximately two orders of magnitude less than a typical graphite/epoxy

composite. Concerns over the mechanical characteristics of such a composite system may arise from because of these stiffnesses. However, it must be pointed out that in the braiding process, a combination of fiber orientations are utilized, similar to the lamination process of conventional composite construction. By having a combination of fiber orientations in the braided construction, the resulting material characteristics can approach those of typical epoxy systems, as will be shown a part of this effort.

The initial testing of the flexible composite construction was on a 9 x 2 x 0.125 in. AS4 graphite braid with a +57° apparent fiber orientation. These samples had approximately 2 inches of each end infiltrated with an epoxy, as was indicated above, to allow for mechanical gripping of the sample during tensile testing. Prior to testing, it was hypothesized that the flexible composite system would initially be very compliant. As the load was applied, the high elongation, low stiffness matrix should allow fiber motion in the direction of the applied load. As these fibers translate, the stiffness would increase because of the increased resistance to motion. This occurs from the increasing stiffness of the high elongation material as well as from the constraint that the fibers have on one another as they reach their crimp angle. This latter characteristic is one that is actually very familiar to all, which manifests itself in conventional fiber forms such as rope. To visualize this, consider a rope which is under no load. The fibers are in some cases relatively loose relative to each other. As a tensile load is applied, the fibers which form the rope tend to align with the loading axis, resulting in a bulk motion which tends to reduce the net section of rope form. Physically, there is an initial elongation of the rope with minimal applied load. With additional load, the described fiber motion occurs, which results in an apparent stiffening of the rope.

The flexible braided construction was placed in an Instron test machine with hydraulic grips and loaded at a rate of 0.05 in./min. A large displacement extensometer was attached to the composite to monitor strain as a function of applied load. Figure 1 shows the stress-strain results of the testing of one of the samples. It should be noted that the stress calculation was determined by dividing the load by the initial cross sectional area. The cross sectional area in the gage section of the sample was actually reduced due to the necking down of this area as increased load was applied. The stress-strain response of the material is generally what was anticipated. Initially, the flexible composite is very compliant. As the load on the composite is increased, the specimen stiffness increases, shown

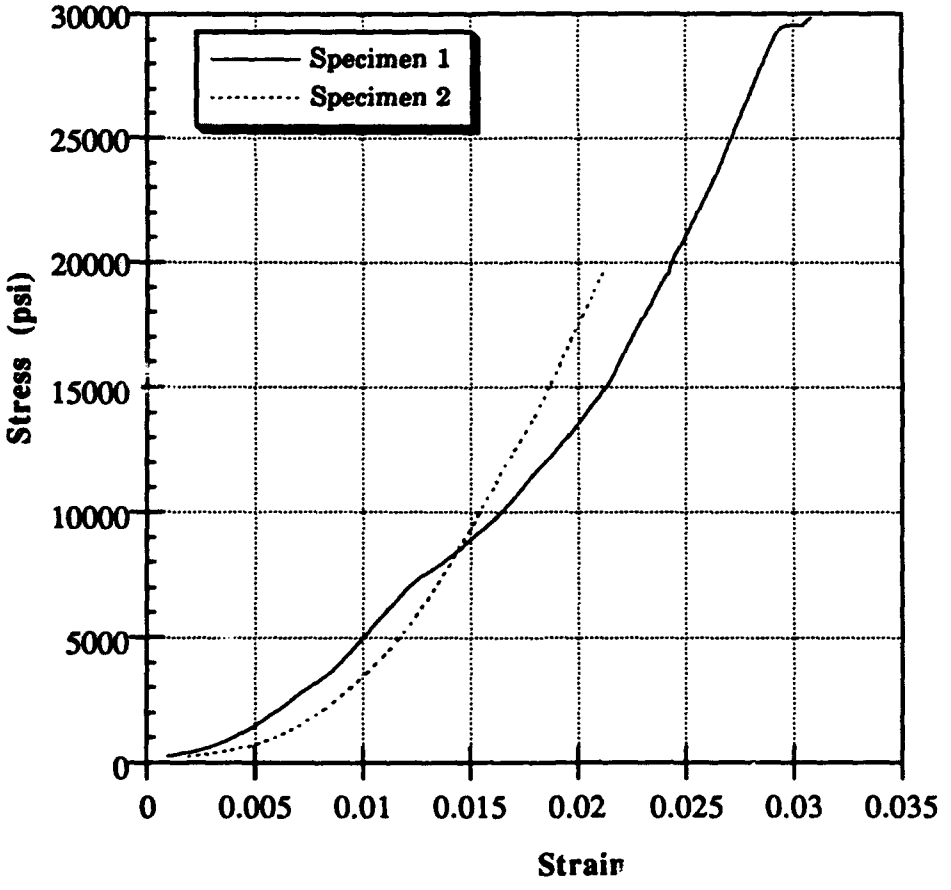

Figure 1: Tensile Stress vs. Strain plot of Braided AS4/REN flexible composite

by the concave up orientation of the stress-strain curve. It should be noted that the specimen was loaded to where the net section stress was approximately 30000 psi. At this point the material began to slip in the hydraulic grips.

From the stress vs. strain plots of both samples, the stiffness as a function of the strain can be determined. This was accomplished by approximating the curves with line segments. The slope of each of these segments are then reported as a function of the maximum strain of each of the line segments. The stiffness as a function of strain can then be plotted. These results are shown in figure 2.

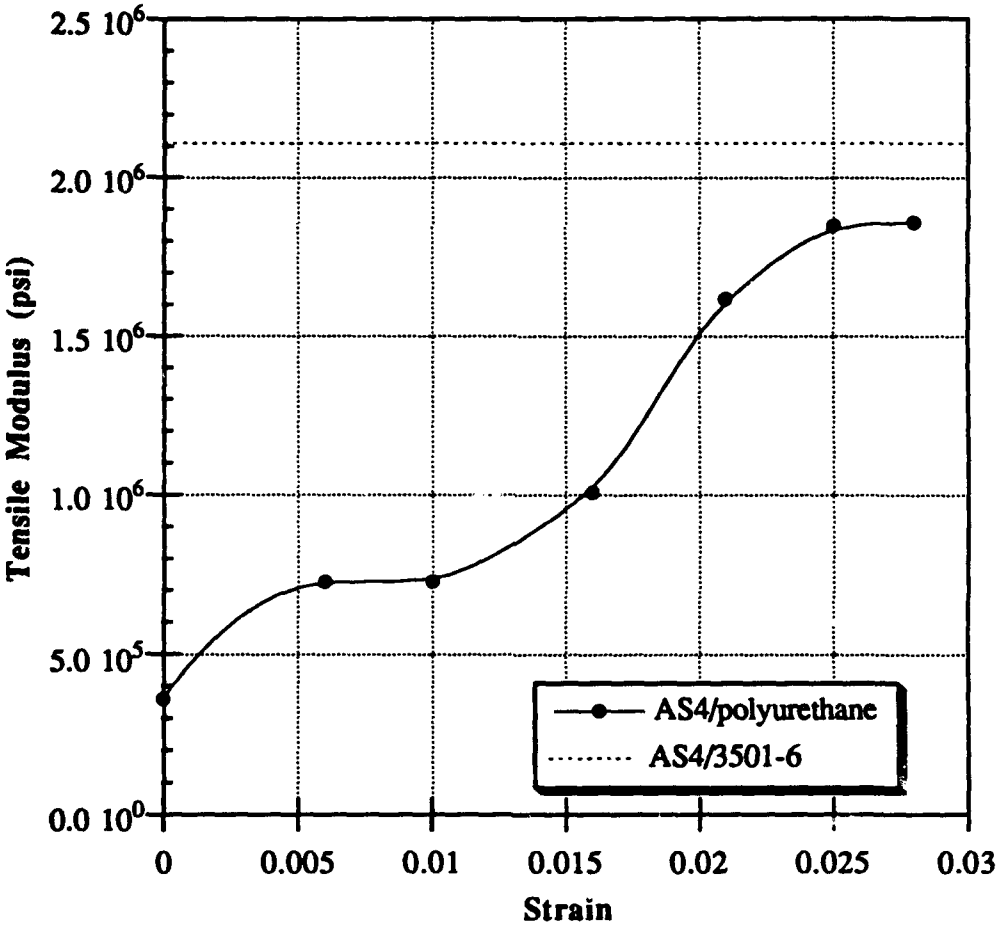

Figure 2 Tensile modulus as a function of strain for the AS4/polyurethane composite material.

The tensile modulus is shown to be initially very low, although significantly greater than the urethane stiffness (1000 psi.). As the specimen is loaded in tension, the modulus shows an initial increase to about 0.7 Msi. As the fibers approach their crimp angle, where they can no longer rotate and there is direct impingement between them, which occurs at about 1.5% strain, the modulus is seen to increase significantly. This increase in modulus eventually approaches an asymptotic value at a strain of approximately 2.5%. The significant point that requires mention is that the asymptotic modulus for the AS4/polyurethane is approximately equal to the value of a graphite/epoxy specimen with the same initial fiber orientation.

This latter point is significant. Through the proper selection of braid pattern, a specific initial fiber orientation can be achieved. The maximum tensile modulus for the specific braid pattern can then be estimated as that of a conventional fiber/polymer matrix composite. In addition to the fiber orientations that result from the braiding process, it is also possible to incorporate fixed axial fibers in the fiber preform. This allows the braided sections to achieve significant torsional and axial stiffnesses with little manufacturing difficulty.

Mechanical Vibration Damping

The flat plate testing of the flexible composite has shown that the material form can support significant loads, possesses a stiffness approaching that of a conventional composite system and is readily manufactured using normal composite RTM techniques. This material also has the potential to provide

significant dissipation of mechanical vibrations. This energy dissipation will occur as a result of the braided configuration and the high damping viscoelastic material used as the matrix for this composite form.

A typical thermoset composite material has mechanical vibration damping characteristics which, like the mechanical properties, are anisotropic. The damping property of the material is typically characterized by an anisotropic damping loss factor, η. Depending on the fiber orientation and layup, the damping loss factor for glass or graphite epoxy composite specimens can be one to two orders of magnitude greater than a structural metal such as steel. (4) The composite high damping loss factor is the result of many loss mechanisms such as the fiber-matrix interface, the loss factor of the matrix, the stress couplings, fiber orientation, and fiber volume fraction.(5) The braided composite configuration with the polyurethane possesses an additional mechanical vibration damping mechanism; constrained layer damping.

In the braided composite form, the fibers form a particular angle relative to the load direction, shown as α in figure 3a. When the material is placed under load, since the matrix is compliant, the fibers which form the braid can move relative to each other to some new angle. Figure 3b shows the relative angular translation of the fibers to an angle of $\alpha + \theta$, when the braid is subjected to a load in the braid direction. This fiber translation subjects the matrix to both a compressive and shear loading. Since the matrix material is chosen for its high damping characteristics and since the energy dissipation of a viscoelastic is most efficient in shear, this material form will possess a high damping loss factor.

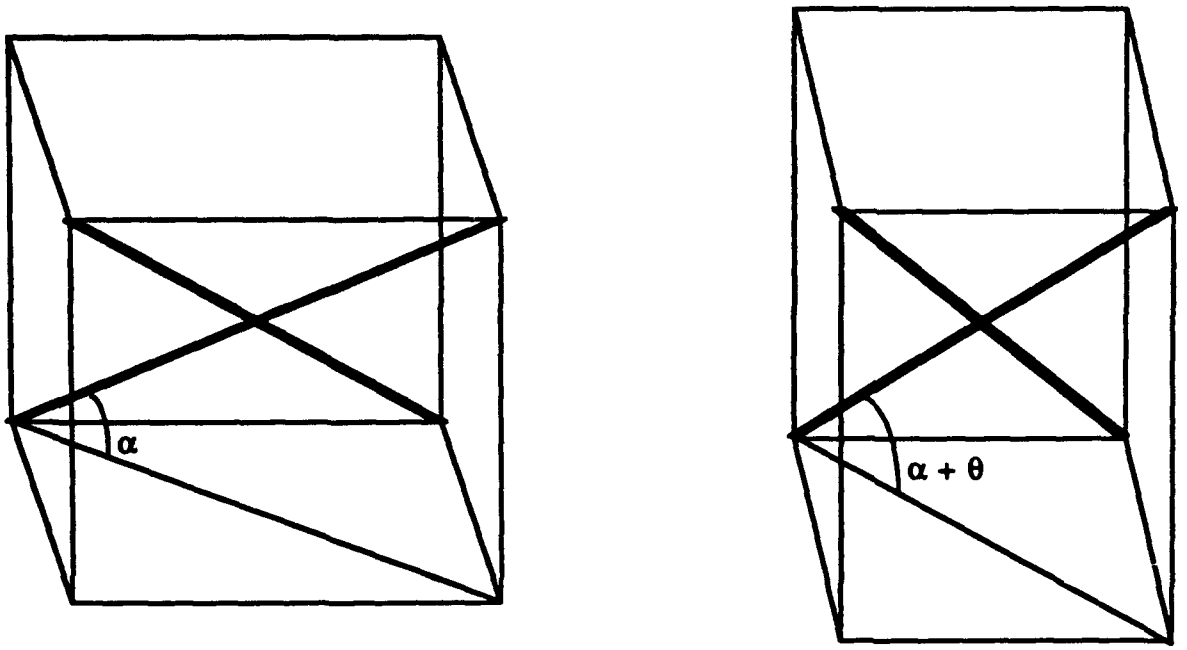

Figure 3 Schematic of unit cell for braided fiber composite form.

To determine the damping loss factor of this material form, test specimens were fabricated. The specimens were identical to the specimens described in the mechanical tests. Specifically, these specimens were 9 x 2 in. with a thickness of 0.125 in. The fibers were AS4 graphite and the viscoelastic material was the REN polyurethane.

The initial tests that were performed were the conventional free-free beam test. Here, the beam is suspended from an isolating support and excited with an impulse excitation. The response is measured with an accelerometer. The damping loss factor is determined using either the half power point method or the reverberation time method. Details of the specific techniques can be found in references 6 and 7, respectively.

The results of the testing are given in Figure 4 for both the reverberation time and half power point methods. It should be noted that both techniques show similar results with the reverberation time method results less than 10% lower than the half power point method. The reverberation time method results are probably more accurate due to the errors associated in the half power point method when the loss factor becomes large, i.e. greater than 0.1.

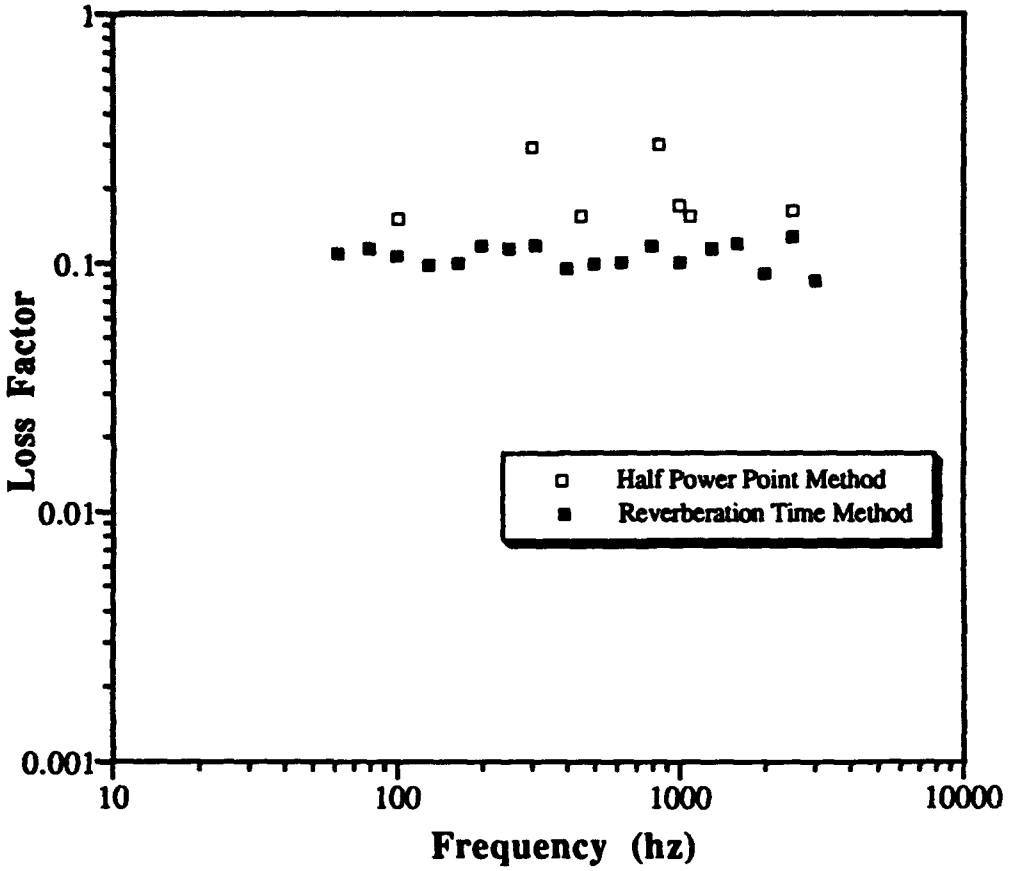

Figure 4 Damping loss factor of AS4 graphite braided composite with polyurethane matrix.

The braided composite with the polyurethane matrix has a loss factor that is approximately an order of magnitude greater than a conventional composite which has a thermoset material such as epoxy or vinylester as its matrix (5).

This is the magnitude of damping loss factor that is desired for many structural applications. In a particular structural configuration, the loss factor of the system will undoubtedly be greater than the test specimen value because of the additional losses which occur at joints and attachments.

Although this material exhibited a loss factor which was significant using the conventional test procedures for determination of material damping loss factor, questions existed regarding the level of damping that the material would provide when it was subjected to a mechanical loading. Determination of the loss factor of this material under load will provide a realistic measure of the performance of this material as it would be utilized in an actual structural configuration. To accomplish this, the loss factor of the material was determined using a different test method. Here, the specimen was initially loaded in tension to a mean load of 500 lb. The specimen was then cycled at $\pm$0.005 in. The damping loss factor was determined using the phase lag analysis, which is an automatic feature of the Instron Test Machine. Details of the phase lag analysis procedure for the determination of the damping loss factor for materials can be found in reference 6. The mean load of the specimen was then increased by 500 lb to 1000 lb. The specimen was again cycled with a displacement of $\pm$0.005 in. The loss factor was determined using the phase lag method. This procedure of increasing the mean load in 500 lb increments and determining the loss factor by cycling the specimen with $\pm$0.005 in. displacement was continued until a load of approximately 3500 lb. At this point, there were audible acoustic emissions, indicative of fiber failure.

The results from the testing are given in figure 5. The results are

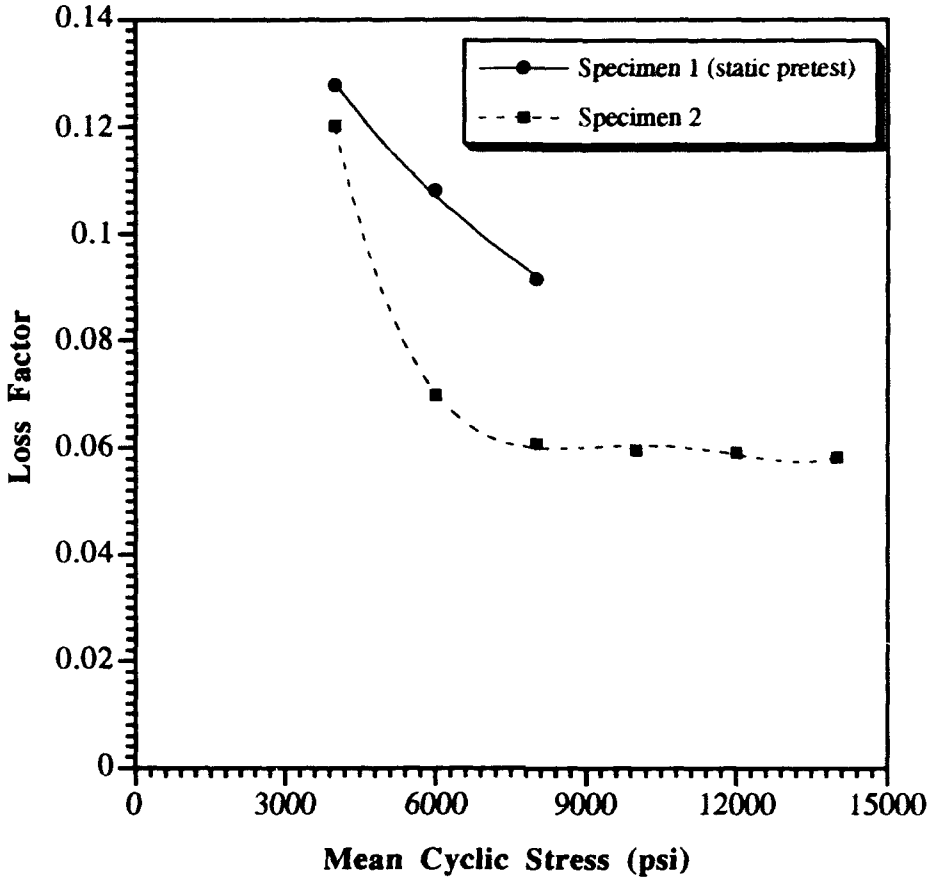

Figure 5 : Loss factor vs. mean cyclic stress for braided AS4 fiber with polyurethane matrix using phase lag analysis

presented as a loss factor at a given mean stress. The mean stress is determined by dividing the load on the specimen by the cross sectional area. The frequency of the test machine was approximately 50 hz for all load increments. The results of the testing are typical of what was expected. The initial damping loss factor of the specimen was approximately the same as that determined using the other test procedures, between 0.1 and 0.2. As the specimen was subjected to increasing loads, the damping loss factor decreased to an asymptotic value of approximately 0.06. It should be pointed out that this damping value is significant, since it can be considered a material damping loss factor for a structural material. If this

type of material were part of a structural system, with joints and attachments, the total system damping loss factor would be greater than this. One could therefore conservatively consider this value to be a lower bound for the loss factor of this system component.

Design and Fabrication of a Flexible Composite Shaft Coupling

Utilizing the results of the coupon testing, a cylindrical shaft coupling was designed. The material form was a braided AS4 graphite fiber preform which was to be infiltrated with a resin transfer moldable polyurethane. The specific shaft coupling had two structural load requirements: a torsional requirement which results in a maximum shear stress of of 8000 psi, and an axial stress of 2000 psi.

A decision was made to fabricate the braided cylindrical shaft coupling using AS4 graphite fibers, the same fibers as were used in the coupon testing. A decision was made, however, to use a different polyurethane. This decision was made because of the flow and cure characteristies of the REN material previously used in conjunction with the requirements necessary for the new fabrication method that was required for the coupling. The systems used was DuPont Adiprene. A comparison of the properties of the Adiprene to the REN urethane are given in Table 3.

With the constituent materials chosen and with knowledge of the design loadings , the fiber orientations and thickness of the cylinder was determined.

	REN	Adiprene
Hardness (Shore A)	60	60 - 90
%Elongation		240 - 450
Tensile Strength (psi)	2000	2000 - 8000
Tensile Modulus psi (at 100%)	500	800 - 4000

Table 3 Material Properties of polyurethane

This was accomplished using a PC based computer program called Cylan (8). This program determines stresses and strains in laminated composite cylinders which are subjected to combined axial load, internal pressure, and torsional shear using a Vlasov-Ambartsumyan type laminated shell theory. This analysis also includes through-the-thickness normal strain effects. The determination of the strength of the laminated shells is performed using a quadratic interaction criteria given in reference 9.

To perform the analysis, the material properties are input in a data file. The material properties were determined using the micromechanical methods given in equations 1-4. The strength predictions were made using conventional micromechanical techniques. Equations 5-7 (9) are the specific equations utilized for the longitudinal tensile strength, σ_1, the transverse tensile strength, σ_2, and the shear strength, τ_{12}.

$$\sigma_1 = \sigma_f V_f + \sigma_m V_m \tag{5}$$

$$\sigma_2 = \frac{\sigma_{mu}}{S} \tag{6}$$

where

$$S = \frac{1 - V_f\left[1 - \frac{E_m}{E_f}\right]}{1 - \left(\frac{4V_f}{\pi}\right)^{\frac{1}{2}}\left[1 - \frac{E_m}{E_f}\right]} \tag{7}$$

$$\tau_{12} = \frac{1 + V_f\left(\frac{1}{\eta_s} - 1\right)}{K_{ms}} S_m \tag{8}$$

where S_m is the matrix shear strength, K_{ms} is the matrix stress concentration factor, and η_s is the shear partitioning parameter which can be determined as

$$\eta_s = \frac{1}{2}\left(1 + \frac{G_m}{G_f}\right) \tag{9}$$

The lamina strengths determined using equations 5-9 are given in Table 4.

	Longitudinal Tensile (ksi)	Longitudinal Compressive (psi)	Transverse Tensile (psi)	Transverse Compressive (ksi)	Shear (psi)
AS4	360×10^3				
Adiprene Polyurethane	4500		4500		
Composite	180×10^3	40000	1820	15000	4000

Table 4: Composite strength properties used in cylinder analysis

The loading that the shaft section will be subjected to is predominantly shear, along with an axial component. In conventional composite design, fiber orientations of 0° and 45° would be the most efficient for supporting these loadings. As such, various combinations of 45° and 0° plies were used in the design for a shaft section. The specific laminate orientation which was analytically shown to satisfy the load requirements was $[45/-45/45/-45/0]_{3S}$. The first ply failure shear strength of this laminate was given to be 8700 psi. This was the fiber orientation that was utilized for the fabrication of the braided shaft section.

A cylindrical braided composite fiber preform with a fiber orientation of $[45/-45/45/-45/0]_{3S}$ was purchased from Atlantic Research Corp. The inner diameter of the cylinder was 2.645 in. with a wall thickness of 0.24 in. The braided composite cylinder required 40 tows through the thickness to make the obtain the necessary wall thickness. The effective layer thickness was 0.006 in.

The resin transfer technique to infiltrate of the braided cylindrical section required experimental development. In addition to conventional requirement of less than 1% void content along with a high fiber volume fraction, the technique had to allow for preferential infiltration of the ends of the cylindrical sections. This was to allow for the mechanical attachment of the cylinders to a metallic coupling. This was necessary based on the results of the flat specimens which showed the inability to mechanically fasten to the polyurethane infiltrated braided sections. The infiltration process also had to allow for the impregnation of the center section of the braided section with a high viscosity polyurethane. The flow characteristics of the polyurethane required the ability to hold a vacuum prior to

infiltration as well as a pressure of 60 psi. during the actual resin transfer of the polyurethane. Because of these characteristics, a simple closed mold was fabricated which would allow for both the epoxy and polyurethane infiltration.

The male mandrel that was used as the mold surface onto which the fiber preform was braided was also utilized as the actual mandrel for the resin transfer process. A section of this mandrel, approximately 16 in. long was cut from the original 42 in. mandrel. A two piece clam-shell mold was then made which had an internal diameter of 3.5 in. which will provided the outer surface for the composite part. This outer mold was used only for the resin transfer of the polyurethane. It should be noted that the internal diameter was greater than the diameter of the braided cylindrical section. This was purposefully done so that during the resin transfer molding process, the maximum surface area of of the braided preform would be used in the infiltration process.

The assembly and process required for the infiltration process with the epoxy was significantly simpler. A schematic of the apparatus utilized is shown in figure 6. The braided preform is initially placed on the 16 in mandrel. A release film is wrapped around the braided composite 3 in. from each end of the preform. A 3 inch width of peel ply material, teflon coated nylon, is wrapped over this release film at each end of the cylinder. This aids in the transfer of the resin into the fiber preform by enabling the resin to flow over the specific fiber surface which will be infiltrated. Once the resin has flowed over the surface, it must only penetrate the thickness of the fiber preform. In the more traditional method of resin transfer molding, there are resin inlet ports positioned at various locations along the part. The resin in this case must flow not only through the thickness

but also throughout the plane of the fiber preform itself in order for the entire section to be filled with resin.

A spiral slit tube is then positioned on the mandrel, in contact with the braided preform end. A solid plastic tube is placed into this slit tube as shown in figure 6. This tube is the resin inlet port for the resin transfer process. A breather cloth is wrapped around the braided preform near the center of its

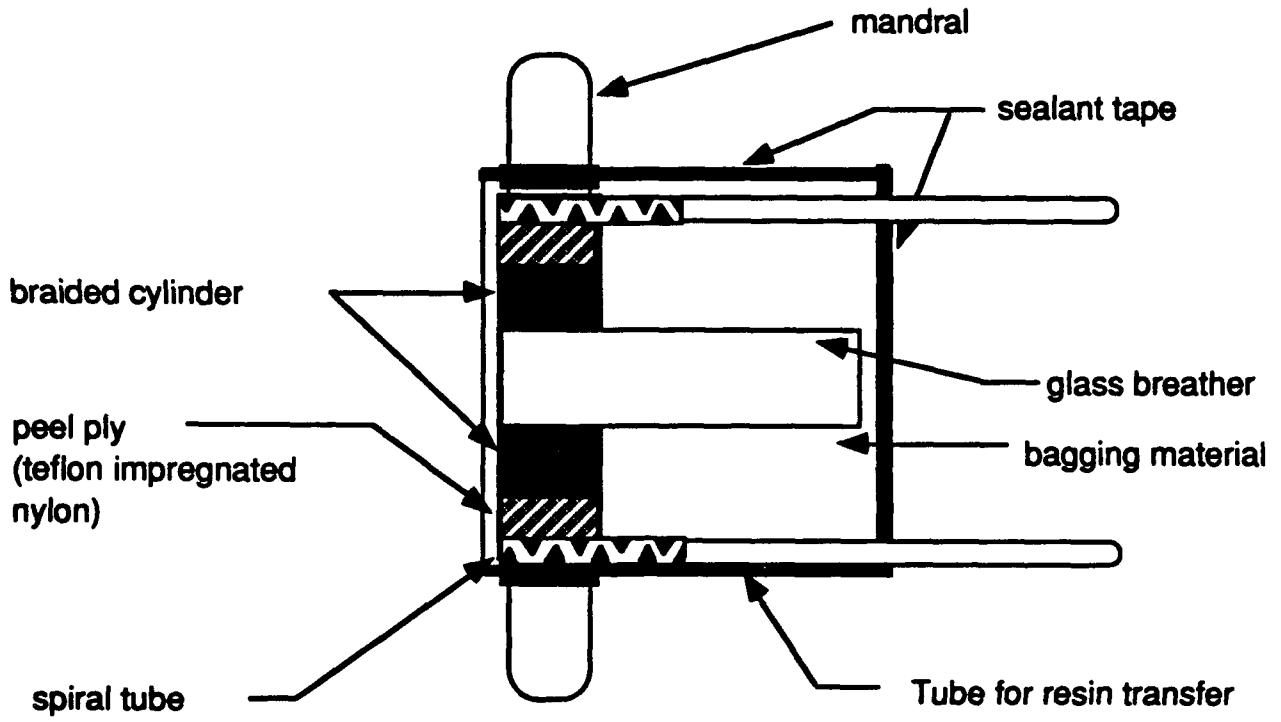

Figure 6 Schematic of assembly used for epoxy resin transfer into braided preform

length, ensuring that it is not in contact with either resin transfer medium material. A vacuum bag is then formed using sealant tape on a mylar film, totally encompassing the assembly. As shown in figure 6, the solid plastic tubes are allowed to penetrate the vacuum bag.

One end at a time is infiltrated with the epoxy resin. The assembly is positioned vertically and the two ends of the tubes which penetrate the vacuum bag are sealed with sealant tape. A vacuum is applied to the assembly, and the integrity determined by removing the vacuum ensuring that it will maintain the vacuum without vacuum pump. After this, the assembly is evacuated for 5 minutes. The resin that will be used for the infiltration is then mixed and placed in a small container. The lower tube is then crimped, the sealant tape removed and the open end placed into the container of resin. Crimping the tube does not allow air to enter the vacuum bag. The tube is then uncrimped and the resin is drawn into the assembly through the tube under vacuum only. The resin is allowed to flow into the tube and the resin front is visually monitored. When the front reaches the top of the peel ply material, the tube is crimped and removed from the resin container. The end of the tube is then sealed with the sealant tape. The assembly is kept in the vertical position under vacuum for 4 hours at which time the opposite end is infiltrated. To do this, the assembly is rotated 180° so that the uninfiltrated end is positioned like the previous section, a shown in figure 6. A container of resin is then mixed. The tube is crimped and its end is placed in the container of resin. The sealant tape is removed, the tube uncrimped and the resin is allowed to flow through the tube and into the braided preform up to the top of the peel ply material. The resin in the preform is then allowed to cure at room temperature for 24 hours. The time required for the resin to flow through the tube, into the fiber preform material, and up approximately 3 inches is about 10 seconds.

After the epoxy ends have cured, the vacuum bag assembly is removed. The resulting mandrel/composite preform is then assembled into a clam shell

mold, shown in figure 7, for infiltration with the polyurethane. This mold assembly consists of 2 aluminum half cylinder pieces and two urethane end plugs. The aluminum pieces have a groove machined into the edge cut region in the axial direction of the cylinder. This is done to accept a rubber o-ring which is necessary so that a seal can be made to maintain both a vacuum and pressure. The mold is held together with C-clamps. All of the interfaces are sealed with silicone RTV to minimize air and urethane leakage. A valve is placed at the inlet and bleed ports to allow for a vacuum to be applied to the assembly and for it to hold pressure during and after the resin transfer process. Flexible tubing is then

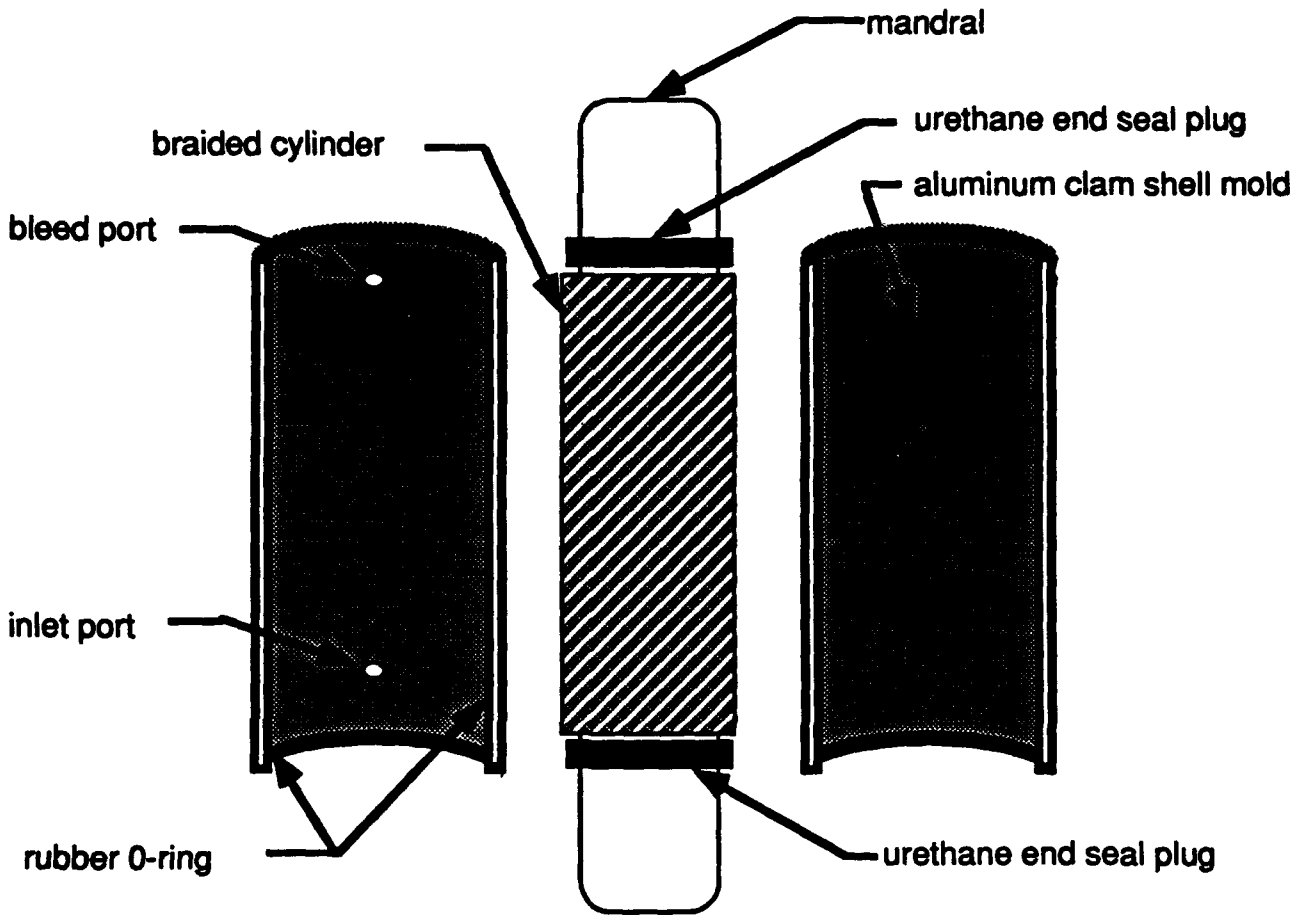

Figure 7 Closed mold used for polyurethane infiltration

attached to these valves. The tubing on the bleed port is to allow for attachment to a vacuum pump as well as to allow for the polyurethane to flow into during the infiltration process. The tubing at the inlet is used to connect the mold assembly to a pressurized infiltration gun.

The assembly is then placed into an oven which has been heated to 140° F. This is required to keep the viscosity of the polyurethane to a minimum after it enters the mold. This maximizes the potential for a complete void free infiltration of the braid section. A pressurized infiltration gun is then attached to one end of the mold assembly. The inlet valve is closed and the bleed valve, which is connect to a vacuum pump, is opened. The mold is evacuated for approximately 5 minutes to assure that there are no leaks. The inlet valve is then opened and the polyurethane is pulled into the mold under the vacuum alone. The vacuum is maintained until the polyurethane flows out of the bleed port and approximately 1 foot into the bleed port tubing. At this point the valve at the bleed port is closed. A pressure of approximately 50 psi. is applied to the polyurethane at the inlet port by the pressure gun. The application of pressure to the gun assures all of the evacuated space is filled with polyurethane, that the braided composite is fully infiltrated and that any voids that may remain are kept to a minimum. This assembly is kept in the oven at temperature and with the applied pressure for approximately 4 hours to fully cure the polyurethane. Afterwards, the assembly is allowed to cool and composite part is removed from the mold.

This infiltration process was used to fabricate two different flexible composite sections. The first was the flexible shaft coupling that was previously mentioned. The second was a flexible pipe coupling. Two different urethanes

were used in these efforts because of the different requirements of each application. In addition, the fiber form was different in both cases. The shaft coupling utilized the multidimensional braided composite preform, whereas the pipe coupling fiber preform was a wrapped fabric. In both cases, there were no problems with the full infiltration of the fiber preforms.

MECHANICAL TESTING OF FLEXIBLE COMPOSITE SHAFT SECTION

The primary loading requirement for a shaft section is to transfer torque. In addition, it must also be capable of supporting a bending moment that may result from misalignment as well as from the shaft loading itself while rotating. The flexible composite shaft section was tested using an existing test facility developed by the Mechanical Transmissions Branch of the Carderock Division Annapolis Detachment of the Naval Surface Warfare Center. This facility has the capability to apply a specified torque while measuring the resultant axial load.

In order to load the flexible composite section in the existing test facility, a flange joint was attached to each end of the shaft section. The specific flange joint configuration consisted of a conventional flange section with a three inch long pipe section attached. The flexible shaft section was manufactured so that it could be inserted, with minimal clearance, over the pipe flange section. To ensure the integrity of the joint during the torsional testing, the composite was both adhesively bonded and mechanically attached to the metallic pipe flange. The adhesive used was Philly Bond TA30 structural epoxy adhesive. The mechanical attachment consisted of a conventional ring fedder shrink disk coupling. This

configuration has been previously utilized in the testing of shaft sections made with conventional composite materials.

The experimental apparatus, shown in figure 8, applies a torque to one end of the shaft section while restraining the opposite end from turning. The fixed end has a load cell attached for determination of the axial load to which the shaft is subjected. The torsional mechanical characteristics are determined using a set of inclinometers which are attached to each of the flanges. The shear modulus of the system can be determined by measuring the torque as a function of the angle of twist.

Figure 8 Experimental apparatus used to torsionally load shaft sections

The shaft was torsionally loaded in 50 ft-lb increments. At each 50 ft-lb loading, the angular deflection of each end of the shaft was recorded. In addition, the axial load at each torque increment was also recorded. For the initial flexible section tested the angular deflection was linear with applied torque up to 400 ft-lb. After reaching this torque, the shaft end where the torque is applied began to rotate without any increase in torsional load. The flexible shaft section reacted to this twist by a torsional buckling mode. This buckling is shown in figure 9. After reaching a relative angular deflection of one end relative to the other of approximately 20°, the shaft was unloaded. After unloading, the buckled area of the shaft returned to its original shape showing no permanent deformation.

Figure 9 Torsional buckling of flexible shaft section loaded to 400 ft-lb

Since there was no external sign of damage, the shaft was reloaded. Again, the torque was applied in 50 ft-lb increments, with the angular deflection and axial load recorded at each loading. When the torque reached 400 ft-lb, the buckling occurred again, resulting in a significant twist of the torsionally loaded end relative to the fixed end, without any increase in the hydraulic pressure for the loading apparatus. At this point, a decision was made to allow the shaft to twist to the maximum allowed by the test machine. This degree of twist was allowed to determine if there was a crimp point for the braided construction as had been seen in the flat panel put under tensile loading. It was felt that there be a degree of twist where the fibers would begin reacting with one another, resulting in an increase in the load carrying capacity of the shaft.

As the machine was allowed to rotate, the shaft section continued to torsionally buckle. The rotation of the machine continued until the maximum was reached, which was approximately 60°. At this point, the machine was unloaded. The shaft again returned to its original shape without any external signs of damage.

The torsional buckling was not anticipated. The critical torque for buckling was therefore analytically determined. The critical torque is defined as

$$T_c = 21.75\,(D_{22})^{\frac{5}{8}}\left(\frac{A_{11}\,A_{22} - A_{12}^2}{A_{22}}\right)^{\frac{3}{8}}\frac{R^{\frac{5}{4}}}{L^{\frac{1}{2}}} \qquad (10)$$

where A_{ij} and D_{ij} are the ij^{th} terms of the laminate stiffness matrices, R is the

radius to the midplane of the material and L is the length of the cylindrical section. Utilizing this equation, the flexible coupling should have a critical torque of 377914 in-lb. In order to utilize this equation, however, the material must satisfy the following inequality,

$$\left(\frac{D_{22}}{D_{11}}\right)^{\frac{5}{6}}\left(\frac{A_{11}A_{22}-A_{12}^2}{12A_{22}D_{11}}\right)^{\frac{1}{2}}\frac{L^2}{R}\geq 500 \qquad (11)$$

Using the material characteristics for the flexible coupling material, the result for the inequality is 55.9. Since the material does not satisfy this inequality, equation 10 is not valid. However, there are no analytical methods available to determine the torsional buckling strength for a material with the mechanical properties of the flexible composite system.

In order to prevent torsional buckling, the interior of the coupling was filled with sand. Since this is a common practice employed for naval shafting, it was felt that torsional testing of the coupling with the sand would result in valid performance information.

The coupling was filled with sand and retested. The applied torque and angle of twist was measured were recorded in 100 ft-lb increments. A decision was made to load the coupling to failure. As the torque was being increased from 1500 to 1600 ft-lb, the adhesive joint failed. The results of the test are shown in figure 10, where the angle of twist if plotted against the value of TL/J, where T is the applied

torque, L is the length of the gage section of the coupling between the joint region, and J is the polar moment of inertia. These results are plotted to determine the

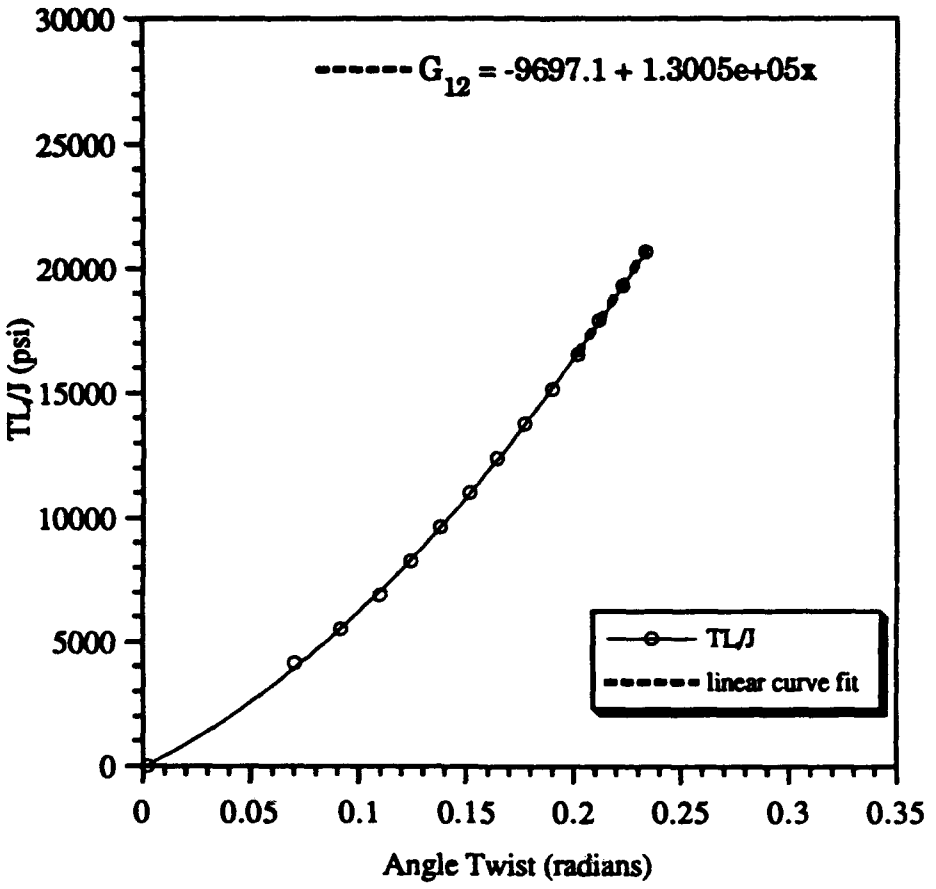

Figure 10 Torsion test results of flexible coupling filled with sand.

shear modulus of the coupling, which is the slope of the curve. The slope of the curve is seen to increase with increasing applied torque. The resultant slope of the curve for the final four data points, with the applied torque ranging from 1200 to 1500 ft-lb, the shear modulus was found to be 0.13 Msi.

It should be pointed out that the coupling loading response did not show any physical signs of imminent failure. There were no audible emissions indicative of fiber failure. Most impressive was the fact that there was no buckling present at the time of the failure of the joint adhesive bond. It appears that the sand provides enough stability to prevent the torsional buckling previously experienced

Since the coupling had still not failed, the decision was made to rebond the coupling to the metallic flange and retest to failure. Again, the coupling was filled with sand to prevent torsional buckling. The shaft was again incrementally loaded to failure. Failure occurred as the torque was being increased from 25200 in-lb to 26400 in-lb. This was approximately 85% of the design goal.

The failure of the coupling was significantly different from that of conventional composite systems. Typically, when a composite is loaded in a mode in which the fibers carry the predominance of the loading, failure is very energetic due to the release of the significant level of energy stored in the material. In the case of the flexible coupling, the failure was significantly different. First there were some audible fiber failures. The sound emitted was much different than that in conventional matrix systems. Instead of the sharp distinct "ping" associated with thermoset composite systems, the sound was more muffled. As more fibers failed, a break on the surface was created. As the applied torque was continued, this surface grew at a 45° angle to the axis of the cylindrical section. The failed fibers protruded from the surface. As this crack was propagating, a second failure surface was created, diametrically opposed to the first. These fiber failures and associated break began at the opposite end of the coupling, again propagating in a 45° direction to the axis of the cylinder. When the angle of twist

reached approximately 30°, the coupling was unloaded. It should be pointed out that the coupling was still intact at this point. A picture of failed coupling is shown in figure 11.

Figure 11 Failed coupling

Although the coupling did not reach the design level expected, the results were very promising. It was felt that the initial loading without the sand where the coupling experienced an angular displacement of approximately 60° caused some fiber failure. Because of this, it was decided to impregnate the second braided shaft coupling with the same urethane material and repeat the tests using sand as a support against torsional buckling.

The same procedure for infiltration and testing was followed the second shaft section. A second one foot long braided fiber preform was cut from the remaining braided material. Again, three inch sections are each end of the braided section

were infiltrated with epoxy using the procedure discuss above and cured. This material was then place in the RTM mold and infiltrated with the Adeprene L100 polyurethane. As such, this shaft section was identical to the first one tested.

The shaft was bonded to the conventional ring fedder shrink disk coupling and was filled with sand. The assembly was placed in the torsion test apparatus to again determine the modulus and strength of the system. In the torsional testing, angle of twist measurements were taken at 100 in-lb increments. In this test piece, the coupling was loaded up to the design load of 30000 in-lb without any sign of buckling or other damage. At this point the coupling was unloaded. The coupling was then cycled to the 30000 in-lb level for four cycles, to see if there were any variations in the load history. There were no noticeable differences.

After the fourth cycle, the coupling was to be loaded to failure. When the loading reached 37000 in-lb, the joint failed. It should be noted that this is 20% over the design goal of 30000 in-lb. The results of this last test are shown in figure 12. The shear modulus near the design load is also shown in figure 12 as the slope of 0.49×10^6 psi. This is approximately double the value obtain for the first coupling at the lower load level.

Since the coupling had shown no signs of degradation, the joint was rebonded so that the coupling could be loaded to failure. For this second test, the angle of twist as a function of torque was again recorded for comparison with the first test. Since this test was to determine the strength of the coupling, the angle of twist vs. torque measurements were recorded only in 6000 in-lb increments from 12000 to

35000 in-lb. After this, this information was recorded at 1200 in-lb increments.

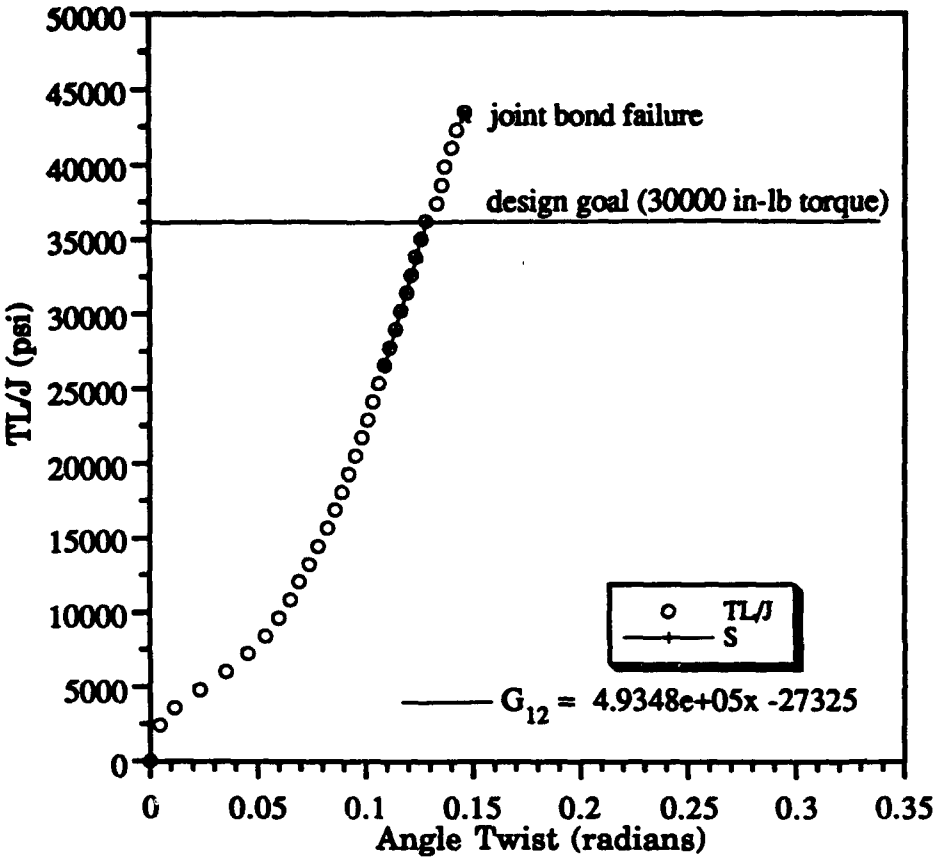

Figure 12 Torsional test results of the second braided coupling

The coupling did not fail until the load was being increased from 58000 to 59000 in-lb. The results of this testing are shown in figure 13.

The results of this testing are very promising. The shear modulus determined at the higher torque levels was approximately 0.41 Msi, which was similar to the shear modulus obtained at torques below the design level. In addition, the failure occurred gracefully, with a gradual increase in angle of twist as the torque was

continually applied. The coupling was allowed to twist until the limit switch was activated, which occurs at an angle of approximately 60°. The two ends of the coupling were still intact after the coupling was removed from the test machine.

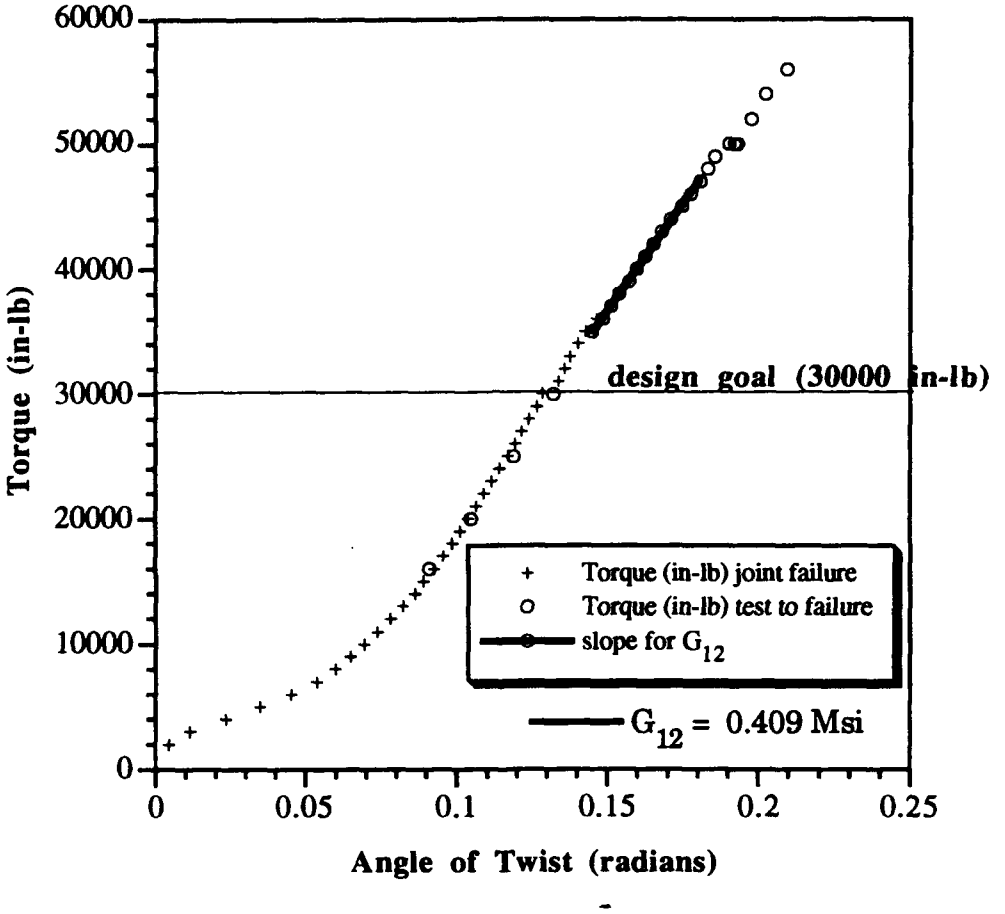

Figure 13 Coupling torsion test to failure

The results of this testing are very promising. The shear modulus determined at the higher torque levels was approximately 0.41 Msi, which was similar to the shear modulus obtained at torques below the design level. In addition, the failure occurred gracefully, with a gradual increase in angle of twist as the torque was continually applied. This is direct contrast to a typical failure of conventional

composite materials where the failure are very energetic, occurring with a sudden release of energy. Most often this is accompanied by significant fiber breakage and delamination. The coupling was allowed to twist until the limit switch was activated, which occurs at an angle of approximately 60°. The two ends of the coupling were still intact after the coupling was removed from the test machine.

With the success of these preliminary results, additional tests are planned. The first is to utilize a different urethane system. The system of choise will be the same Adiprene polyurenthane but with a different curative. This material combination will result in a reduction in hardness, from a Shore A of approximately 100 to a Shore A of 60. This is accompanied by a similar reduction in elastic modulus. These results will be presented in a future paper.

Axial Damping Test Method

In addition to providing a flexible coupling capable of transferring torque while subjected to a misalignment, it was assumed that the use of the polyurethane matrix should provide significant attenuation of vibrational energy. The primary mode of transmission of energy along shaft sections is through axial vibration. These vibrations are transmitted to the shaft from the machinery to which it is attached, and can be transmitted to other portions of the ship hull, equipment or the surrounding medium. The shaft sections that were fabricated for structural testing were therefore also tested to determine the damping that they provide. An assessment of their performance was attempted by comparing the response of several shaft sections ranging from conventional steel to an experimental

conventional composite design.

In this program, only the axial damping characteristics were determined. To couple axial vibrations into the cylindrical sections, heavy end caps were secured to each end of the shaft section. These end caps serve two purposes. First, they provide a good distribution of the applied excitation force from a mechanical shaker across the whole pipe circumference. Additionally, and perhaps more importantly, they provided a significant inertia compared to the mass of the shaft. In this way the shaft material tends to act as a spring, with an inertia at each end. As a result, the vibration is mechanically amplified near resonance, enabling better damping estimates to be made.

To isolate the shaft section from the surroundings, they were suspended horizontally using light steel cables. The axial excitation was applied at one end using an inertial electrodynamic exciter. The force excitation and acceleration response were measured with a calibrated impedance head built in to the exciter. The excitation signal was pseudo random, in the frequency ranges 0-5 kHz and 0-2 kHz (depending on the material), and signals were captured and converted to accelerance with a Hewlett Packard 3562A Signal Analyzer. The resulting data were transferred to PC for analysis purposes as well as for ease in graphing and comparison with theoretical data.

THEORY

The testing methodology that was used experimentally determines the response of

the test system to the axial excitation. The system not only includes the material to be interrogated but also includes the specific end constraints utilized. To obtain the material loss factor from the specific testing conditions required the utilization of an analytical model which would be capable of determining the material response using the experimental modal response of the shafts.

Classic vibration theory was used to determine an undamped theoretical model which included both discrete and continuous elements. This was then extended to include hysteretic damping by making the stiffness term complex. The full expansion of the equations is extensive, and is not necessary for a good curve fit. Therefore an intermediate simplification for wave speed is made and used to solve for the material loss factor.

The analysis treats the shaft as a continuous system, with a discrete mass at each end. The transfer function for each component is determined as follows:

For end cap mass m_1 with external forcing F_0 and internal reaction force from the pipe F_1 the free body diagram is:

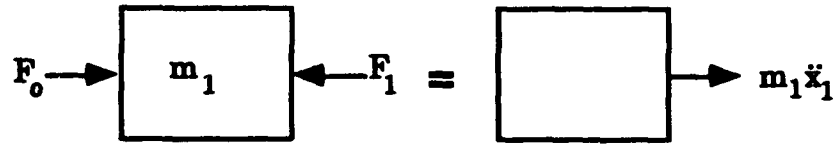

Figure 14 Free Body diagram for mass m_1

From the free body diagram, the force response and displacement can be written

as :

Similarly, for mass m_2 $\begin{vmatrix} x_1 \\ f_1 \end{vmatrix} = \begin{vmatrix} 1 & 0 \\ \omega^2 m_1 & 1 \end{vmatrix} \begin{vmatrix} x_1 \\ f_o \end{vmatrix}$ the force response and displacement can be written as :

$$\begin{vmatrix} x_2 \\ f_3 \end{vmatrix} = \begin{vmatrix} 1 & 0 \\ -\omega^2 m_1 & 1 \end{vmatrix} \begin{vmatrix} x_2 \\ f_2 \end{vmatrix}$$

It should be noted that the external forcing function f_3 is zero for this experiment.

The shaft is considered to be a continuous system. Newton's Third Law means forces f_1 and f_2 from the masses are applied to the ends of the shaft. Assuming harmonic compression waves travel along the shaft, and making the classic assumptions for compression waves in prismatic bars, a solution is assumed for the longitudinal displacement at any section to be of the form

$$u(x,t) = \left(C \sin\left(\frac{\omega x}{c}\right) + D \cos\left(\frac{\omega x}{c}\right)\right) \sin(\omega t) \qquad (14)$$

where C and D are constants defined by the boundary conditions, and the velocity of compression waves in the pipe, c, is given by

$$c = \sqrt{\frac{E}{\rho}} \qquad (15)$$

At $x = 0$

$$f_1 = -EA\frac{\partial u}{\partial x} \tag{16}$$

from which

$$C = \frac{f_1 c}{EA\omega} \tag{17}$$

At x = L (the length of the pipe)

$$f_2 = \frac{EA\omega}{c}\left(C\cos\left(\frac{\omega L}{c}\right) - D\sin\left(\frac{\omega L}{c}\right)\right) \tag{18}$$

hence

$$D = -\frac{f_2 c}{EA\sin\left(\frac{\omega L}{c}\right)} - \frac{f_1 c}{EA\omega}\frac{\cos\left(\frac{\omega L}{c}\right)}{\sin\left(\frac{\omega L}{c}\right)} \tag{19}$$

Substituting values for C and D gives

$$x_1 = u(0,t) = -\frac{f_1 c}{EA\omega\tan\left(\frac{\omega L}{c}\right)} - \frac{f_2 c}{EA\omega\sin\left(\frac{\omega L}{c}\right)} \tag{20}$$

$$x_2 = u(L,t) = -\frac{f_1 c\sin\left(\frac{\omega L}{c}\right)}{EA\omega} - \frac{f_1 c\cos\left(\frac{\omega L}{c}\right)}{EA\omega\tan\left(\frac{\omega L}{c}\right)} - \frac{f_2 c}{EA\omega\tan\left(\frac{\omega L}{c}\right)} \tag{21}$$

The transfer matrix between the ends of the pipe can therefore be written in the form

$$\begin{vmatrix} x_2 \\ f_2 \end{vmatrix} = \begin{vmatrix} \frac{b_2}{a_2} & \left(\frac{b_2 a_1}{a_2} - b_1\right) \\ -\frac{1}{a_2} & -\frac{a_1}{a_2} \end{vmatrix} \begin{vmatrix} x_1 \\ f_1 \end{vmatrix}$$

with

$$a_1 = \frac{c}{EA\omega \tan\left(\frac{\omega L}{c}\right)} \tag{23}$$

$$a_2 = \frac{c}{EA\omega \sin\left(\frac{\omega L}{c}\right)} \tag{24}$$

$$b_1 = \frac{c \sin\left(\frac{\omega L}{c}\right)}{EA\omega} + \frac{c \cos\left(\frac{\omega L}{c}\right)}{EA\omega \tan\left(\frac{\omega L}{c}\right)} \tag{25}$$

$$b_2 = \frac{c}{EA\omega \tan\left(\frac{\omega L}{c}\right)} \tag{26}$$

Combining the transfer matrices and simplifying the equations results in

$$\begin{vmatrix} x_2 \\ f_3 \end{vmatrix} = \begin{vmatrix} 1 & 0 \\ -\omega^2 m_2 & 1 \end{vmatrix} \begin{vmatrix} \frac{b_2}{a_2} & -\frac{c \sin\left(\frac{\omega L}{c}\right)}{EA\omega} \\ -\frac{-EA\omega \sin\left(\frac{\omega L}{c}\right)}{c} & -\frac{a_1}{a_2} \end{vmatrix} \begin{vmatrix} 1 & 0 \\ -\omega^2 m_1 & 1 \end{vmatrix} \begin{vmatrix} x_1 \\ f_0 \end{vmatrix}$$

Applying the condition that f_3 is zero yields

$$\frac{x_1}{f_0} = \frac{\left(\cos\left(\frac{\omega L}{c}\right) - \frac{c\,\omega^2 m_2 \sin\left(\frac{\omega L}{c}\right)}{EA\omega} \right)}{-\omega^2 m_2 \cos\left(\frac{\omega L}{c}\right) + \frac{\omega^4 m_1 m_2 c \sin\left(\frac{\omega L}{c}\right)}{EA\omega} - \frac{EA\omega \sin\left(\frac{\omega L}{c}\right)}{c} - \omega^2 m_1 \cos\left(\frac{\omega L}{c}\right)}$$

This equation gives the receptance (displacement per unit force) of the pipe structure with end cap masses, with both the excitation and response being measured at the same end mass. Hysteretic damping can be included by making the elastic modulus complex. This effects both the modulus and wave speed terms in the above equation, viz:

$$E^* = E(1 + i\eta)$$

$$c^* = \sqrt{\frac{E(1 + i\eta)}{\rho}}$$

The sine and cosine functions have complex arguments, and should be expanded as

$$\cos\left(\frac{\omega L}{c^*}\right) = \cos(a + ib) = \left[\frac{e^b + e^{-b}\cos(a)}{2}\right] + i\left[\frac{e^{-b} - e^b \cos(a)}{2}\right]$$

However, for small damping the wave speed is nearly real, and for this investigation it was kept as the real number. The wave speed is therefore given as

$$c = \sqrt{\frac{E(1 + \eta^2)}{\rho}}$$

The equation for receptance can now be separated into real and imaginary parts. This procedure generates large equations, which is not necessary to show here. However, included in Appendix A is the Visual BASIC subroutine which was used to calculate the receptance function, converts the receptance to accelerance, and returns the real, imaginary, modulus and dB modulus values of accelerance. It should be noted that for this report, some of the long lines of code are printed on 2 lines, which is actually an invalid format for Visual BASIC.

Damping Results and Discussion

Four different shaft materials were tested as part of this investigation to quantify the damping and level of vibration isolation provided by the flexible composite material form compared with some more conventional material systems. The systems investigated included a conventional steel, a baseline composite the design of which had been previously tested, a high damping shaft section from the Lord Corporation and the flexible composite fabricated as part of this effort. The baseline composite shaft section was a hybrid design, which used layers of glass/epoxy and graphite/epoxy in a base laminate configuration. The base laminate configuration is $[(90_2/\pm 45)_{glass}(\pm 45)_{3carbon}]_s$ which was filament wound by Hercules Corp. The Lord Corporation high damping shaft was a glass fiber reinforced polyurethane. Details on the fabrication and material components were not disclosed.

Prior to the dynamic tests, the static Young's Modulus of elasticity was measured since this value is a required input parameter in the analytical model. The modulus was obtained by loading the ends of the cylinder using flat plates and

measuring the strain using an extensometer in the gage section. These value were used as the initial value when comparing experimental dynamic data with theoretical values. The results of the compression testing are shown in Table 5.

Material	Compression Modulus (psi)	Max. Load (lb)	Cross-Sectional Area (in^2)
Steel	31.88×10^6.	5992, 5971	3.162
Baseline Composite	2.44×10^6	1400, 1407, 1409	2.879
Lord (Damped Composite)	0.234×10^6	1396, 1400, 1612	3.194
Flexible Composite	1.637×10^6	1000, 1258, 1416	2.074

Table 5 Axial compression test results for damping tests on shaft sections

BASELINE STEEL SHAFT

Length	0.946 m
Cross Sectional Area	0.00199 m^2
Density	7843 kg/m^3
End cap mass (each)	4.0 kg
Static Young's Modulus	219.8×10^9 N/m^2
Dynamic Young's Modulus	210.0×10^9 N/m^2
First Longitudinal Resonance	1,813 Hz
Loss Factor (this model)	0.19 %
Loss Factor (modal analysis)	0.09 %

The original aim of testing the steel shaft was to verify the accuracy and suitability of the test method. In actuality, the steel shaft was the most difficult to analyze, and results were inconclusive. This was for several reasons. The primary reason is because of the theoretical analysis of the rig. The rig was

designed and analyzed assuming the longitudinal (compression) vibrational waves were reflected at the boundary between the end of the shaft and the attached end caps. This seems to work satisfactorily when the shaft and end caps are significantly different materials (i.e. the wave speeds are very different). However, when both the shaft and end caps are made of steel, wave reflection is not so effective. The only way this analysis gave a reasonable result was to include part of the length of the end caps in the overall length of the shaft. This predominantly effected the estimate of Young's Modulus.

An overlay of the measured and theoretical frequency response functions is shown in Figure15. Wave motion and reflection in the end caps may also explain the measured double peaks near 1,800 Hz and 3,500 Hz, although this may also be a measurement problem associated with the very low levels of damping in steel.

Another problem with the design for the steel shaft was that the end cap mass required to get the fundamental resonance below about 1 kHz was so high that it was impractical. Smaller end caps had to be used, making the frequency that much higher, and above those for the composite shafts.

BASELINE COMPOSITE SHAFT

Length	0.718 m
Cross Sectional Area	0.00186 m^2
Density	1726 kg/m^3
End cap mass (each)	3.15 kg
Static Young's Modulus	16.82 x 10^9 N/m^2
Dynamic Young's Modulus	19.0 x 10^9 N/m^2
First Longitudinal Resonance	860 Hz
Loss Factor (this model)	1.9 %
Loss Factor (modal analysis)	1.8 %

This shaft was the easiest to analyze, and confidence in the results is high. An overlay of the measured and theoretical FRFs is shown in figure 16.

FLEXIBLE COMPOSITE SHAFT - EMPTY

Length	0.1397 m
Cross Sectional Area	0.01338 m^2
Density	4012 kg/m^3
End cap mass (each)	3.44 kg
Static Young's Modulus	11.29 x 10^9 N/m
Dynamic Young's Modulus	11.20 x 10^9 N/m
First Longitudinal Resonance	1,217 Hz
Loss Factor (this model)	2.62 %
Loss Factor (modal analysis)	2.59 %

The curve fits for this shaft were very good. An overlay of the measured and theoretical FRFs is shown in figure17. Confidence in the results for this shaft is high.

FLEXIBLE COMPOSITE SHAFT - SAND FILLED

For this experiment the hollow shaft was filled with 1.7 kg of dry white sand. The original shaft was 7.66 kg with end caps (0.75 kg without end caps), making a mass ratio of sand to shaft of 0.22 (2.27 ignoring end caps). Despite adding a significant mass to the structure, the frequency of the first longitudinal resonance was only slightly reduced and was essentially unchanged. The change was of similar order to the experimental error.

The only significant change was in loss factor. Adding sand significantly increased the loss factor from 2.6% to 4.8%.

LORD DAMPED COMPOSITE SHAFT

Length	0.911 m
Cross Sectional Area	0.0023 m^2
Density	1432 kg/m^3
End cap mass (each)	0.54 kg
Young's Modulus	1.613×10^9 N/m^2
First Longitudinal Resonance	438 Hz
Loss Factor (this model)	8.5 %
Loss Factor (modal analysis)	3.2 %

The curve fit for this shaft was very good, and is shown in Figure 18. Unfortunately, the loss factor as estimated by modal analysis and this theoretical model is significantly different. In an attempt to verify which value was more appropriate, the loss factor was also estimated using the half-power point method.

This gave a loss factor very comparable to that estimated by modal analysis. This suggest the Lord damped shaft is not behaving as expected by the theoretical model, but no apparent reason was found.

SENSITIVITY

A detailed sensitivity analysis was not undertaken. The following are presented as discussive items only.

The natural frequencies generated by the theoretical model are highly sensitive to shaft cross sectional area. For the steel shaft the cross sectional area was calculated from the shaft's mass and length, and the density of steel. For the composite shafts, the density was calculated from the mass, length and cross sectional area. The areas were calculated from measured inside and outside diameters. Undoubtedly much of the variation in results is attributable to inaccuracies in the effective cross sectional area.

As expected, the natural frequencies depend on the Young's Modulus of the material, but the variation is not as marked as that observed for a variation in cross sectional area.

Variation of the end cap mass has very little effect on natural frequencies, and since the masses were know accurately (within less than 0.5% for most caps) inaccuracy in this value has little impact on the results.

CONCLUSIONS

Structurally, the braided composite preform infiltrated with a high strain to failure matrix, polyurethane, is capable of sustaining significant loading in both tension and torsion. When failure occurs, the event is atypical of conventional composite materials. The material fails gracefully, and does not exhibit the typical sudden release of energy associated with destruction of surfaces. Instead, the release of energy is gradual, showing a gradual decrease in the load carrying capacity and an increase in the global deformation of the part. As a material system, the flexible braided composite structure is suitable for shaft coupling applications.

The quadratic failure theories for determination of the shear strength are inadequate for this material form. The Tsai-Wu first ply failure stress in shear was determined to be aproximately 8700 psi. The shear stress at failure from the torsion test was approximately 19200 psi. In addition, classical laminated plate theory is inadequate for determination of the shear modulus of the flexible composite. The value obtained experimentally, 0.41 Msi is approximately an order of magnitude lower than the analytical value of 3.6 Msi. It should be noted, however, that the tensile properties analytically determined using classical laminated plate theory and progressive failure provided a very satisfactory estimate of the experimentally determined values, within 10%.

A methodology for determining the axial dynamic properties (Young's Modulus and damping) of the various composites was developed. A test rig was designed to

amplify motion by resonating in the frequency range of interest. This was achieved by loading the ends with masses (the end caps). The method was successful, and is recommended for any further investigation.

Comparison of the loss factor estimated with this method and by modal analysis is excellent for the baseline composite and flexible composite shafts. For the baseline steel and Lord damped composite shafts, this method produced loss factors about twice those estimated from modal analysis. The steel shaft was the lightest damped shaft, and the Lord damped shaft compared to the flexible unit with sand filling. Therefore it appears this uncertainty does not depend on the level of damping.

A cross check using the half power point method concluded that the modal analysis method was more reliable for determination of the damping loss factor for these shafts than the theoretical model used here.

The estimates of dynamic Young's Modulus show that the composite moduli are essentially independent of frequency.

The magnitude of Young's Modulus is best determined from a static (or very low frequency) test, and the complex component (loss factor) is best determined by modal analysis on a resonant test rig.

Acknowledgements

The authors would like to acknowledge the support of Joe Korczynski and Minor Appleman for their support in the testing of the shaft couplings, and Dave Johnson and James McDonnell for their support in the impregnation of the braided material with the polyurethane and the bonding of the composite to the metallic flanges.

References

1. Brown, Richard T. and Crow, Eddie, C., Jr., "Automated Through-The-Thickness Braiding," Proceedings of the 37th International SAMPE Symposium, 9-12 March, Anaheim, Ca., pp. 832 - 842.

2. Crane, R.M. and Camponeschi, E.T., Jr., "Experimental and Analytical Characterization of Multidimensionally Braided Graphite/Epoxy Composites", Experimental Mechanics, Vol.26, No.3, September 1986, pp. 259-266.

3. Jones, Robert M., Mechanics of Composite Materials, Hemisphere Publishing Corporation, New York, 1975

4. Crane, Roger M., "Vibration Damping Response of Composite Materials," DTRC-SME 91/12, April 1991, 228 p.

5. Crane, Roger M., Gillespie, John W., Jr., and Pipes, R. Byron, "Literature Review of the Vibration Damping Characteristics of Continuous Fiber Organic Matrix Composites," The University of Delaware, Center for Composite Materials Report, CCM-87-35, December 1987

6. Read, B.E. and Dean, G.D., The Determination of Dynamic Properties of Polymers and Composites, Halsted Press Book, 1978.

7. "Damping of Vibrations in Graphite/Epoxy Structures", NASA Tech Briefs No. MFS-27228, George C. Marshall Space Flight Center, March 1979, 196 p.

8. Whitney, James M. and Gillespie, J.W., Jr., Cylan Cylinder Analysis, Center for Composite Materials, College of Engineering, University of Delaware, Newark, De., August 1984

9. Tsai, Steven, and Thomas Hahn, Introduction to Composite Materials, Technomic Publishing Co., 1980

Appendix A Visual BASIC program to calculate accelerance of the pipe

```
Sub frf (w As Single, rpart As Single, ipart As Single, dbmag As Single)
Dim denom As Double
Rem need the following:
Rem ym = Young's Modulus (real)
Rem d  = volumetric density
Rem n  = loss factor
Rem l  = length
Rem m1 = end mass
Rem m2 = end mass
Rem w = omega (rad/s)
Rem a = cross-sectional area of pipe
Rem factors etc
c = Sqr(ym * Sqr(1 + n ^ 2) / d)
cs = Cos(w * l / c)
sn = Sin(w * l / c)
ay = a ^ 2 * ym ^ 2
n1 = (n ^ 2 + 1)
n2 = (n ^ 2 - 1)
n4 = (n ^ 4 + 2 * n ^ 2 + 1)
f1 = ay ^ 2 * n4 - a ^ 2 * c ^ 2 * w ^ 2 * ym ^ 2 * (m1 ^ 2 * n1 + 4 * m1 * m2 + m2 ^ 2 *
     n1) + c ^ 4 * m1 ^ 2 * m2 ^ 2 * w ^ 4
f2 = 2 * a * c * w * ym * (m1 + m2) * (ay * n1 - c ^ 2 * m1 * m2 * w ^ 2) * sn * cs
f3 = (ay * (2 * m1 + m2 * n1) - c ^ 2 * m1 ^ 2 * m2 * w ^ 2) * cs ^ 2
f4 = c * m1 * w * (ay * n2 + c ^ 2 * m1 * m2 * w ^ 2)
Rem Denominator follows
denom1 = (f1 * cs ^ 2 - f2 - ay ^ 2 * n4 - c ^ 2 * m1 * m2 * w ^ 2 * (2 * ay * n2 + c ^ 2 *
     m1 * m2 * w ^ 2))
Rem Real part receptance follows
rpart = (c * w * f3 + a * ym * (ay * n1 - c ^ 2 * m1 * w ^ 2 * (m1 + 2 * m2)) * sn * cs +
     f4)
rpart = rpart * c / denom1 / w
Rem Imaginary part receptance follows
ipart = -a * c * n * ym * sn * ((ay * n1 - c ^ 2 * m1 ^ 2 * w ^ 2) * cs - 2 * a * c * m1 * w
     * ym * sn) / denom1 / w
' convert to accelerance
rpart = -w ^ 2 * rpart
ipart = -w ^ 2 * ipart
rmag = Sqr(rpart ^ 2 + ipart ^ 2)
dbmag = 20 * Log(rmag) / Log(10)
End Sub
```

INITIAL DISTRIBUTION

Copies

12 DTIC

4 NAVSEA
- 1 05M3 (Pinto)
- 1 55Y2 (Provencher)
- 1 55Y2 (Will)

PEO-SUB-R
- 1 (Spero)
- 1 (Dozier)

2 NRL
- 1 6383 (Badaliance)
- 1 6383 (Wolock)

1 NSWC
- 1 R31 (Augl)

5 ONR
- 1 1132SM (Rajapakse)
- 1 1216 (Vasudevan)
- 1 1131S (Fishman)
- 1 1132SM (Barsoum)
- 1 1132SM (Jones)

2 ONT
- 1 225 (Sloter)
- 1 233 (Remmers)

1 ARPA
- 1 (MSTO) (Kelly)

3 NSWC, White Oak
- 1 Messick
- 1 Garrett
- 1 Grande

1
Dr. Michael L. Drake
University of Dayton
Research Institute - JPC 33
300 College Park
Dayton, Oh 45469

1
Dr. D. Wilkins
Center for Composite Materials
University of Delaware
Newark, DE 19716

CENTER DISTRIBUTION

Copies	Code	Name
1	0114	Becker
1	0115	Caplan
1	0112	Douglas
1	1240	Swanek
1	60D	Krenzke
1	602	Martin
1	65	Rockwell
1	65.1	Tinley
1	65.1	Mayes
1	65.2	Phyillaier
1	69.1(UERD)	Costanzo
1	66.2	Critchfield
1	70	Sevik
1	7022	Maidanik
1	7024	Feit
1	7023	Blake
1	74	Montroll
1	74	Maga
1	74	Fisher
1	741	Warwick
1	741	Cole
1	744	Gershfeld
1	823	Wilhelmi
1	823	Appleman

Copies

1
Dr. Ron Gibson
Mechanical Engineering Dept.
Wayne State University
2140 Engineering Building
Detroit, Michigan 48202

25
Dr. Colin Ratcliffe
U.S. Naval Academy
Dept. of Mechanical Engineering
Annapolis, MD 21402

1
Dr. Martin J. Pechersky
APL/Penn State University
Box 30
State College, Pa. 16804

1
Bruce Sandman
NUSC
Code 8215, Building 679
Newport, RI. 02841

1
Mr. Jack Woods
Foster Miller
350 Second Avenue
Waltham, MA 02154

1
Kevin L. Smith
Dept. E78, Building 600
Newport News Shipbuilding Co.
4101 Washington Ave.
Newport News, VA. 23607

1
Dr. Richard Norton
Science and Technology Dept.
Hercules, Inc.
Research Center, 8136-T6
Wilmington, De. 19894

1
Dr. J. R. Vinson
Dept. of Mech. Engineering
Spencer Laboratory
Univ. of Delaware

CENTER DISTRIBUTION

Copies	Code	Name
Newark, DE 19716		
1	842	Lu
1	60	Wacker
1	601	Morton
25	601	Crane
1	603	Cavallaro
1	612	Wong
1	64	Fischer
1	642	Jones
1	644	Castelli
1	6233	Gallagher
1	522.2	TIC (A)
1	522.1	TIC (C)
1	5231	Office Services

1
Capt. Richard Brynsvold
U.S. Army
Tank Automotive Command
Code AMSTA-RTC
Warren, MI 48397-5000

1
Dr. R.Byron Pipes
President
Rensalier Polytechnique University
NY

1
John M. Winter, Jr.
Center for Nondestructive Evaluation
102 Maryland Hall
The Johns Hopkins University
Baltimore, MD 21218

1
Charles Zanis
CASDE Corporation
2800 Shirlington Road
Suite 600
Arlington, VA 22206

1
Mark Lamontia
I.E. Dupont de Nemours & Co., Inc.
Composites Division
Chestnut Run Plaza
P.O. Box 80702
Wilmington, DE 19880-0702

1
Bob Kolec
Westinghouse
Mail Stop EC-1
401 East Hendry Ave, Box 3499
Sunnyvale, Ca. 94088-3499

1
Dr. Charles Bersch
Institute for Defense Analysis
801 N. Beauregard Street
Alexandria, VA 22311

1
Dr. Donald Flaggs
Lockheed Missiles & Space Co.
ORG 93-30 Building 251
3251 Hanover St.
Palo Alto, CA 94304-1187

1
Dr.John W. Gillespie, Jr.
Assistant Director, CCM
Composites Manufacturing Science Laboratory
University of Delaware
Newark, DE 19716

1
Dr. Roy McCullough
Director, CCM
Composites Manufacturing Science Laboratory
University of Delaware
Newark, DE 19716

1
Dr. Robert E. Green
Materials Science and Engineering
102 Maryland Hall
The Johns Hopkins University
Baltimore, MD 21218

1
George Leon
Electric Boat Division
General Dynamics
Mail Stop J11-431
Eastern Point Road
Groton, CT 06340

1
Longin Greszczuk
McDonnell Douglas Space Systems Co.
Mail Stop 13/3
5301 Bolsa Avenue
Huntington Beach, CA 92647

1
Lowell Smith
Newport News Shipbuilding
& Drydock Company
4101 Washington Avenue
Newport News, VA 23607

1
Dennis L. Blunier
Caterpillar Inc.
Structures;Composites;Simulation
Advanced Materials Technology
Tech. Ctr.
P.O. Box 1875
Peoria, Illinois 61656-1875

1
Joseph S. Boyce
Foster-Miller, Inc
350 Second Ave.
Waltham, MA. 02154-1196

1
Dr. Ronald B. Bucinell
Materials Science Corp.
930 Harvest Drive
Union Meeting Corporate Center
Blue Bell, Pa. 19422

1
Daniel E. Bullock
Foster-Miller, Inc
350 Second Ave.
Waltham, MA. 02154

1
Ed Crow
Atlantic Research Corp.
5945 Wellington Rd.
Gainsville, Va. 22065

1
Dr. Anthony J. Vizzini
Associate Professor & Director
Composite Research Laboratory
Dept. of Aerospace Engineering
University of Maryland
College Park, Md. 20742